Supplemental material for Christian et al., 2021: A probabilistic framework for quantifying the role of anthropogenic climate change in marine-terminating glacier retreats

John Erich Christian[1,2], Alexander A. Robel[2], and Ginny Catania[1]

[1]Institute for Geophysics, University of Texas at Austin
[2]School of Earth and Atmospheric Sciences, Georgia Institute of Technology

Correspondence: John Erich Christian (johnerich.christian@austin.utexas.edu)

1 Model equations and parameters

We use a flowline model solving the 1-D Shallow-shelf approximation for ice flow. This assumes that flow is dominated by longitudinal stretching and basal sliding, and the stress balance is:

$$\rho_i g h \frac{\partial s}{\partial x} = \frac{\partial}{\partial x}\left(2hA^{-\frac{1}{n}}\left|\frac{\partial u}{\partial x}\right|^{\frac{1}{n-1}}\frac{\partial u}{\partial x}\right) - C|u|^{m-1}u. \tag{1}$$

This equation expresses how driving stress (left-hand side) is balanced by a combination of longitudinal stretching (right-hand, first term) and basal drag (right-hand, second term). ρ_i is the density of ice, g is acceleration due to gravity, h is local ice thickness, and $\partial s/\partial x$ is the surface slope. u is the horizontal ice velocity, and A and n are the Glen flow coefficient and exponent, respectively. C and m are the sliding coefficient and exponent, respectively, which here assume a Weertman-type sliding relationship.

The evolution of local ice thickness h is expressed by a continuity equation,

$$\frac{\partial h}{\partial t} = S - \frac{\partial (uh)}{\partial x}, \tag{2}$$

where S is the local surface mass balance.

The terminus is assumed to always be at flotation, and thus the thickness boundary condition there is

$$h_f = -\frac{\rho_w}{\rho_i} b(x_g), \tag{3}$$

where ρ_w is the density of seawater, and $b(x_g)$ is the (negative) bed elevation at the terminus position. We assume the terminus is not buttressed by an ice shelf, and so following Schoof (2007), the velocity boundary condition at the terminus is

$$2A^{-\frac{1}{n}}\left|\frac{\partial u}{\partial x}\right|^{\frac{1}{n-1}}\frac{\partial u}{\partial x} = \frac{1}{2}\rho_i g\left(1 - \frac{\rho_i}{\rho_w}\right). \tag{4}$$

The inland boundary is assumed to be an ice divide where horizontal velocity is zero.

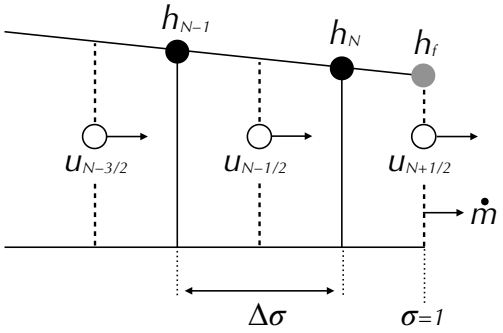

Figure S1. Schematic diagram for numerical grid near the grounding line. Velocities are solved at grid points marked by open circles. Thickness is solved via the continuity equation at grid points marked by black circles, and via the flotation condition at the gray point. The continuity equation thus requires interpolating u to the h grid to calculate flux divergence. For the point h_N, this also includes a flux term from frontal ablation ($\dot{m}$).

We follow the numerical implementation described in detail in Schoof (2007). The thickness (h) and velocity (u) equations are scaled to a grid from $\sigma = 0$ to $\sigma = 1$, where the grounding line always corresponds to the grid point at $\sigma = 1$. The grid thus stretches with grounding-line variations. The h and u grids are staggered such that the last u-grid point corresponds to the grounding line, and the last h-grid point where thickness is solved from the continuity equation is a half grid spacing (i.e., $\Delta\sigma/2$) upstream from the grounding line. However, the grounding line thickness h_f is also solved at $\sigma = 1$ via the flotation condition (Fig. 1).

The equations are solved using finite differences with an implicit time step. The continuity equation (Eq. 2) is discretized with an upwind scheme. Schoof (2007) provides a full description of the numerics. However, one difference from Schoof (2007) is that we have added frontal ablation at the terminus, described as follows and illustrated in Fig. 1. Generally, flux divergence at a thickness gridpoint i is discretized as

$$\frac{\partial}{\partial x}(hu) \sim \frac{h_i(u_{i-1/2} + u_{i+1/2}) - h_{i-1}(u_{i-3/2} + u_{i-1/2})}{2\Delta\sigma}. \tag{5}$$

Note that u must be interpolated because of the staggered grid, both at the thickness point i and its "upwind" point $i-1$. At the last thickness grid point ($i = N$), there is an extra term in the output flux to account for the frontal ablation rate $\dot{m}$:

$$\frac{\partial}{\partial x}(hu) \sim \frac{h_N\big(u_{N-1/2} + u_{N+1/2} + \dot{m}\frac{h_f}{h_N}\big) - h_{N-1}\big(u_{N-3/2} + u_{N-1/2}\big)}{2\Delta\sigma}. \tag{6}$$

Note that because it is assumed to occur at $N + 1/2$ where the thickness is h_f (Fig. 1), it must be scaled by $\frac{h_f}{h_N}$. This frontal ablation is a very general flux anomaly at the terminus. Its effect is to require additional input flux to the the last grid point to balance the continuity equation. Because the terminus is constrained to be at flotation, this results in a steeper surface slope just upstream of the terminus.

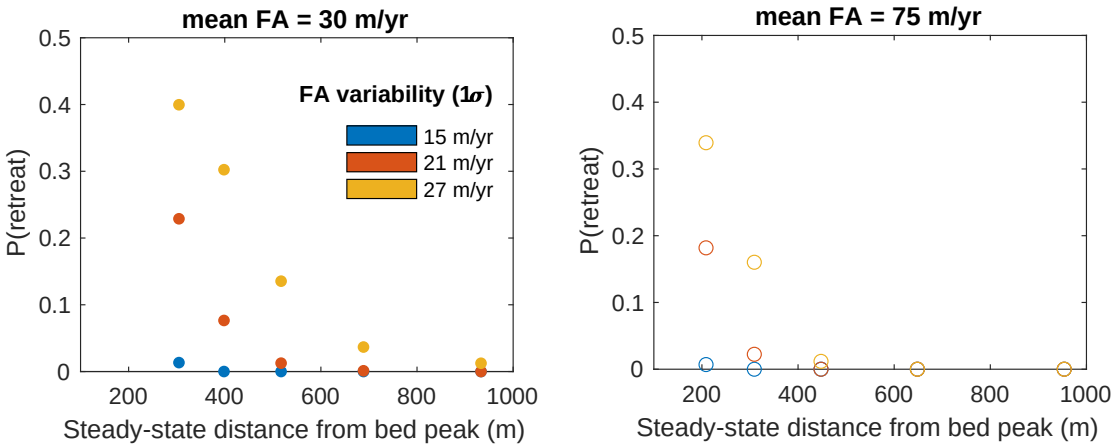

Figure S2. Ensemble retreat probabilities across variations in bed-peak height (which affect the steady-state distance from the bed peak) and the amount of frontal ablation variability. a) Results for the original idealized glacier, which has mean frontal ablation of 30 m/yr, meaning that the lower bound of zero frontal ablation truncates some anomalies, especially for greater σ_{FA}. b) as for a), except for a glacier with mean frontal ablation of 75 m/yr, which minimizes the effect of the zero bound. In either case, however, increasing σ_{FA} can have a large effect on the probability of retreat.

2 Effect of different frontal ablation assumptions

Throughout our experiments, we impose frontal ablation anomalies drawn from distributions with $\sigma_{FA} = 12$–27 m/yr, but in the numerical model we stipulate a lower bound of zero absolute frontal ablation. This avoids numerical issues associated with adding ice at the terminus. However, it means that the most extreme negative anomalies are truncated, and the variability is more asymmetric for greater σ_{FA}. Compared to a symmetric distribution of frontal ablation anomalies, this increases the time-mean of frontal ablation, and therefore moves the time-mean of the terminus fluctuations inland (i.e., closer to the bed peak in our idealized geometry). In principle, this affects the probability of retreat from the bed peak. Thus, our analysis in Fig. 3 of the main text does not fully separate the two effects of proximity to the bed peak and magnitude of variability upon the probability of retreat, because increasing the magitude of σ_{FA} also pushes the glacier closer to the bed peak, on average.

To assess this effect, we also considered a glacier with a higher mean frontal ablation (75 m/yr), so that the zero-bound plays little role for the same range of σ_{FA}. That is, for the strongest variability of $\sigma_{FA} = 27$ m/yr, the lower bound on variability is approximately 2.8σ. To compensate for higher frontal ablation while still yielding a similar steady-state terminus position, we uniformly raised the entire bed with respect to sea level (approximately 60 m), bed kept the dimensions of the bed peak the same with respect to the surrounding topography.

We compare the retreat probabilities in perturbed parameter ensembles for these two glaciers, adjusting the bed-peak height to change the steady-state terminus position (Fig. S2). Panel (a) shows results from the original glacier (i.e., a subset of results from Fig. 3c of the main text), while panel (b) shows results for the glacier with higher mean frontal ablation. Note that the

steady-state distances from the bed peak (and the relation between bed-peak *perturbations* and this distance) are not exactly the same between glaciers. However, the general results are the same: proximity to the bed peak and the magnitude of climate variability are clear controls on the probability of retreat. Thus, while a zero-bound on frontal ablation may contribute slightly to the increased probability of retreat as σ_{FA} is increased, it appears the main effect of larger σ_{FA} is simply the addition of larger perturbations.

We also note that other nonlinearities may also affect the mean terminus position as variability is introduced or increased (Robel et al., 2018). These issues have to be considered when initializing any simulation with noisy forcing, and are in part why we include a transient spinup period in our simulations.

3 Synthetic attribution experiments for a range of parameters

Here we provide additional synthetic attribution analyses with different parameter choices. This helps illustrate the range of probabilities that might be encountered in ensemble experiments, as well as the amounts by which an anthropogenic forcing trend changes the probability of retreat. Frontal ablation trends are applied over the full 150-year experimental interval, and except where noted, the glacier geometry and parameters are as described in the main text.

First, we consider consider a glacier with a higher bed peak (94 m) in order to lower the null probability of rapid retreat (the simulations in Fig. 5 of the main text assumed a bed peak of 90 m) . We apply the same σ_{FA} and Δ_{FA} as in the main text (18 m/yr and 24 m/yr, respectively), with Δ_{FA} applied over the entire 150-year simulation. The trend increases the probability of retreat to approximately 0.5 (Fig. S3a). Such a case would constitute a strong probabilistic attribution statement, since rapid retreat is very unlikely ($P < 1\%$) in the absence of a trend, and thus the multiplier on probability is large. However, that only 50% of simulations produce rapid retreat even with the trend indicates that retreat is still partially contingent on internal variability.

As an alternative case, we consider stronger natural variability ($\sigma_{FA} = 24$ m/yr) and 90 m bed peak, which increase the null probability of retreat to approximately 0.25 (Fig. S3b). A trend of $\Delta_{FA} = 32$ m/yr (giving the same ratio of Δ_{FA}/σ_{FA}) increases the retreat probability to 0.81. This is still a marked increase—more than tripling the likelihood of rapid retreat—but is distinct from a case where rapid retreat is nearly impossible without a trend.

Finally, to generalize further, we aggregate results from multiple ensembles in Fig. S4. Probability of retreat is plotted against the magnitude of the forcing trend, with colors denoting different assumptions about the magnitude of variability and the time of onset of the trend. In all cases, the probability of retreat tends towards unity as Δ_{FA} increases. However, differences in σ_{FA} (blue, red, and yellow markers) affect how rapidly the probability increases (and its baseline in the absence of a trend). Additionally, a trend concentrated in the last 50 years (purple markers) is again seen to increase the probability of retreat less than the early-onset trends.

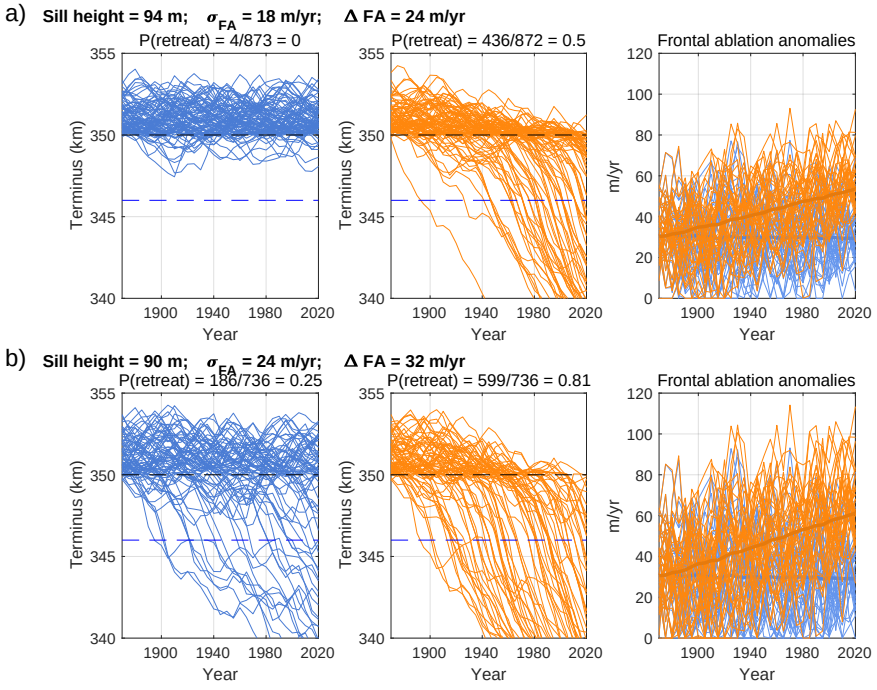

Figure S3. Synthetic attribution experiments with different parameter choices (compare to Fig. 5 in the main text). For clarity, not all simulations are plotted. Left panels show simulations with no trend, center panels show simulations with an anthropogenic trend, and right panels show the frontal ablation anomalies for both scenarios. a) Simulations assuming a slightly higher bed peak, yielding a lower null probability of rapid retreat, and significantly increased probability due to the frontal ablation trend. b) Simulations assuming stronger stochastic frontal ablation variability, yielding higher null retreat probability. A frontal ablation trend still increases the probability of retreat, though by a lesser fractional amount.

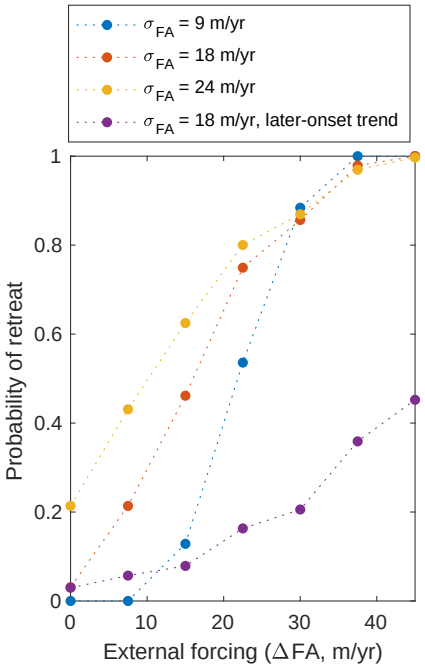

Figure S4. Retreat probabilities from 28 ensemble simulations with different frontal ablation variability and trends. Results are plotted against the total frontal ablation trend, with colors corresponding to differences in the variability or trend onset as indicated. Purple markers correspond to trends applied only over the last 50 years of the 150-year experimental interval; all others assume a 150-year trend.

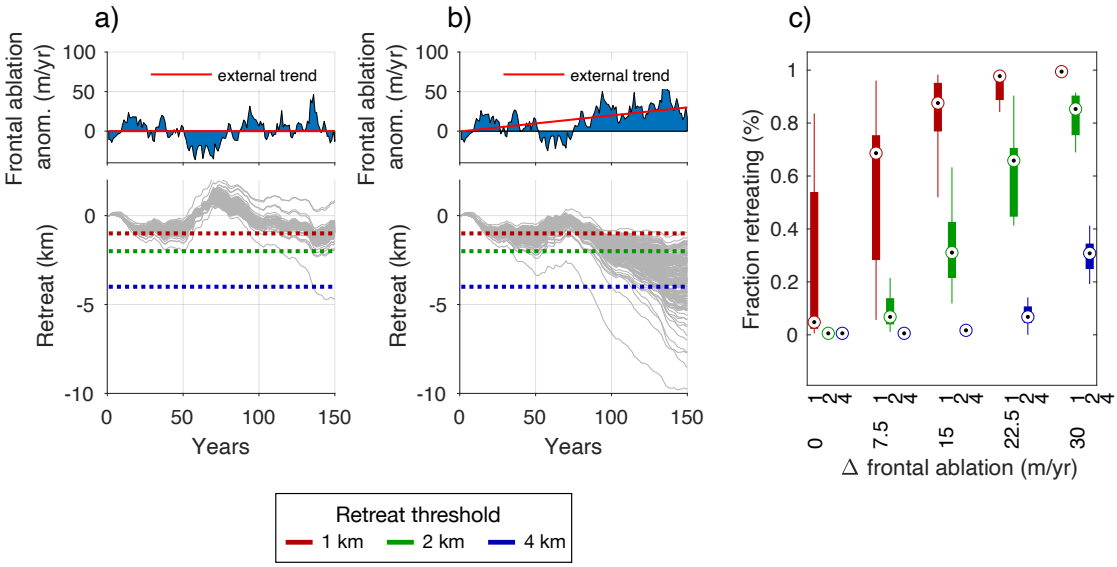

Figure S5. Simulations for the population of glaciers (compare to Fig. 7 of main text). (a) Terminus change (relative to year 0) for each glacier, all forced with the same frontal ablation anomalies (top), which have no external forcing trend. Dashed lines show retreat thresholds. (b) as for (a), except with an external forcing trend in frontal ablation, with a total increase of 30 m/yr over 150 years. (c) Box plot showing proportion of glaciers in the population exceeding the retreat threshold, across six trend scenarios. "Δ frontal ablation" refers to the total linear trend over 150 years. For each level of forcing trend, 20 simulations of the glacier population are run with different realizations of climate variability, with the distribution of retreats indicated with box-and-whisker markers for each retreat threshold.

20

4 Alternative retreat metrics for population of glaciers

In Fig. S5, we show the same synthetic attribution experiment for the population of glaciers as in the main text (Fig. 7), but with multiple retreat thresholds (1, 2, and 4 km). Because each glacier has a different proximity to the closest bed peak (see Fig. 6c), a single retreat threshold applied to the population is somewhat arbitrary. The fraction of glaciers counted as retreating depends on the threshold for retreat, but considering multiple thresholds shows that fraction increases with higher forcing trends regardless of threshold (Fig. S5c).

Code availability. Code for the flowline glacier model is available at https://doi.org/10.5281/zenodo.5245271, and additional scripts for the ensemble analysis and figures are available in a public repository at https://github.com/johnerich/XXXX (will be added in final version).

References

Robel, A. A., Roe, G. H., and Haseloff, M.: Response of Marine-Terminating Glaciers to Forcing: Time Scales, Sensitivities, Instabilities, and Stochastic Dynamics, Journal of Geophysical Research: Earth Surface, 123, 2205–2227, https://doi.org/10.1029/2018JF004709, 2018.

Schoof, C.: Ice sheet grounding line dynamics: Steady states, stability, and hysteresis, Journal of Geophysical Research: Earth Surface, 112, https://doi.org/10.1029/2006JF000664, 2007.